Paper ID: MS-01

In–Situ Synthesis of Ferrites Nano Particles using Sonochemical Route

P. P. Goswami[1], H.A. Choudhury[2], S. Chakma[1,*] and V. S. Moholkar[1]
[1]Department of Chemical Engineering, [2]Center for Energy
Indian Institute of Technology Guwahati
Guwahati – 781039, Assam, India
* *E–mail: sankar@iitg.ernet.in*

Abstract

This paper reports the additives free sonochemical synthesis of manganese ferrite and cobalt ferrite nano–particles using metal acetate as precursors. The synthesis of the ferrites occurs in three steps, viz. hydrolysis of acetates, oxidation of hydroxides and in–situ micro–calcination of metal oxides, and these are facilitated by physical and chemical effects of cavitation bubbles. The collisions between metal oxide particles induced by shock waves generated by transient cavitation are able to cross the activation energy barrier leading to formation of ferrites. The analysis of experimental result showed that $MnFe_2O_4$ and $CoFe_2O_4$ are found to be in nano scale, with uniform morphology and well crystalline nature. Thus, sonochemical route is one of the facile and environmental friendly techniques for synthesis of ferrite nano–particle.

Keywords: *Manganese ferrite, Cobalt ferrite, Ultrasound, Cavitation.*

1. Introduction

Metal ferrites or spinel ferrites nano–particles are one of the most interesting research areas due to their extra ordinary properties and their applications such as magnetic sensors, medical implants, watches, transformer circuits, generator, telecommunications, magnetic fluids and magnetic resonance imaging, microwave absorbers and similar other applications [1–3]. In the last few decades, numerous scientists have reported various conventional techniques for synthesis of metal nano–particles, such as: sol–gel method [4,5], micro–emulsions [6,7], reverse micelles [8], auto–combustion [9] and co–precipitation [10]. Recently few papers are published which dealt with sonochemical route for synthesis of ferrite nano–particles [11–14], in which the reaction mixture is exposed to ultrasound irradiation to provide a required activation energy to overcome the barrier to form ferrites. In sonochemical synthesis of ferrites, acetate metal salts are hydrolyzed followed by oxidation of ferrous hydroxide and the reaction of two metal oxides.

In this study, we have tried to emphasize the links between chemistry of ferrite synthesis and physics of ultrasound and cavitation bubbles by coupling the experimental results with numerical simulations of cavitation bubble dynamics. In sonochemical route, Fe_2O_3 is formed in two step reactions: (i) hydrolysis of iron acetate and (II) oxidation of ferrous hydroxide by H_2O_2 generated by transient collapse of cavitation bubbles. Another effect of ultrasound is the shockwaves which helps the particles of metal oxide to undergo in–situ calcinations in reaction mixture itself due to highly energetic collisions between them induced by it. During the transient collapse, the temperature and pressure inside the bubble reach extremely high, approximately 5000 K and 500 bar respectively. At these extreme conditions of the bubbles, these particles can also undergo in–situ micro–calcination in the thin liquid shell surrounding the bubble where the temperature reaches very high [15–17]. The general mechanism of ferrite synthesis using sonochemical method is as follows [Eqn. 1-6]:
Generation of oxidizing species through sonolysis of water:

$$H_2O \longrightarrow {}^{\bullet}OH + {}^{\bullet}H \quad (1)$$

$$2\,{}^{\bullet}OH \longrightarrow H_2O_2 \quad (2)$$

Hydrolysis of metal acetate to form their respective hydroxide and oxides:

$$Fe(CH_3COO)_2 + 2\,H_2O \longrightarrow Fe(OH)_2 + 2\,CH_3COOH \quad (3)$$

$$X\,(CH_3COO)_2 + 2\,H_2O \longrightarrow XO + 2\,CH_3COOH + 2\,H_2O \quad (4)$$

Where, X represents the metals either Mn or Co. Then the ferrous hydroxide again undergoes a reaction to form its oxide by reacting with H_2O_2 generated by transient collapse of the cavitation bubble. Consequently, the two metal oxides, XO and Fe_3O_4 can react to form XFe_2O_4 through the following reaction) to form.

$$3\,Fe(OH)_2 + H_2O_2 \longrightarrow Fe_3O_4 + 4\,H_2O \quad (5)$$

$$2\,Fe_3O_4 + 3\,XO \xrightarrow{[O]} 3\,XFe_2O_4 \quad (6)$$

For this present study, XFe_2O_4 is the representative of $MnFe_2O_4$ and $CoFe_2O_4$.

2. Materials and methods

Materials: The following chemicals were used for synthesis of ferrites nanoparticles: iron (II) acetate (AR Grade, Sigma–Aldrich), manganese acetate (AR Grade, Sigma–Aldrich), cobalt acetate (AR Grade, Sigma–Aldrich), HCL (AR Grade, Merck), NaOH (pellets form, Merck). All the chemicals were used as received from the suppliers.

Methods: In 20 mL de–ionized water, a 0.2 M of manganese acetate or cobalt acetate was prepared with 0.4 M of iron (II) acetate. Then the reaction mixture was sonicated for 30 min in pulse mode (20 s on 5 s off) using an ultrasonic probe (13 mm OD, 20 kHz) driven by micro–processor controlled unit (Model: VCX500, 500 W). The probe was operated at 20% amplitude with theoretical power dissipation of 100 W. The temperature of the reaction mixture was maintained at 70°C (±4°C) during all the experiments. The pH of the solution was controlled by drop–wise addition of either 0.1N HCl or 0.1N NaOH solution. One should be noted that, there was no addition of external H_2O_2 to the reaction mixture during the synthesis of ferrite nano–particles, as required for the oxidation of ferrous hydroxide. Moreover, no external calcination was employed to the obtained solid products after the sonication.

Numerical modeling of cavitation bubble dynamics: The physical and chemical effects induced by ultrasound and cavitation bubbles in the system were estimated using the diffusion limited ordinary differential equation (ODE) model with boundary layer approximation proposed by Toegel et al. [18]. This model is basically derived from the comprehensive partial differential equation (PDE) model of Storey and Szeri [19], which demonstrated that vapor entrapment in the cavitation bubble, leading to formation of radicals is essentially a diffusion limited process. The main components of the model are set of 4 ODEs as follows: (1) Keller–Miksis equation for the radial motion of the bubble [20]. (2) Equation for the diffusive flux of water vapor and heat conduction through bubble wall. (3) Overall energy balance treating the cavitation bubble as an open system. For greater details readers may see our previous papers [21,22]. The set of 4 ODEs are also given below [Eqn. 7-18]:

1. Radial motion of the cavitation bubble:
$$\left(1-\frac{dR/dt}{c}\right)R\frac{d^2R}{dt^2}+\frac{3}{2}\left(1-\frac{dR/dt}{3c}\right)\left(\frac{dR}{dt}\right)^2 = \frac{1}{\rho_L}\left(1+\frac{dR/dt}{c}\right)\left(P_i-P_t\right)+\frac{R}{\rho_L c}\frac{dP_i}{dt}-4\nu\frac{dR/dt}{R}-\frac{2\sigma}{\rho_L R} \quad (7)$$

Internal pressure in the bubble:
$$P_i = \frac{N_{tot}(t)\,kT}{\left[4\pi\left(R^3(t)-h^3\right)/3\right]} \quad (8)$$

Pressure in bulk liquid medium:
$$P_t = P_0 - P_A\sin\left(2\pi ft\right) \quad (9)$$

2. Diffusive flux of water molecules:
$$\frac{dN_W}{dt} = 4\pi R^2 D_W \left.\frac{\partial C_W}{\partial r}\right|_{r\,=\,R} \approx 4\pi R^2 D_W \left(\frac{C_{W,R}-C_W}{l_{diff}}\right) \quad (10)$$

Instantaneous diffusive penetration depth:
$$l_{diff} = \min\left(\sqrt{\frac{RD_w}{|dR/dt|}}, \frac{R}{\pi}\right) \quad (11)$$

3. Heat conduction across bubble wall:
$$\frac{dQ}{dt} = 4\pi R^2\lambda\left.\frac{\partial T}{\partial r}\right|_{r=R} \approx 4\pi R^2\lambda\left(\frac{T_0-T}{l_{th}}\right) \quad (12)$$

Thermal diffusion length:
$$l_{th} = \min\left(\sqrt{\frac{R\kappa}{|dR/dt|}}, \frac{R}{\pi}\right) \quad (13)$$

4. Overall energy balance:
$$C_{V,\,mix}\,dT/dt = dQ/dt - P_i dV/dt + \left(h_W - U_W\right)dN_W/dt \quad (14)$$

Mixture heat capacity: $C_{V,\,mix} = \sum C_{V,\,i}N_i$ (where, i = N_2/O_2/H_2O)
(15)

Molecular properties of water: Enthalpy: $h_w = 4kT_o$
(16)

Internal energy:
$$U_w = N_w kT\left(3+\sum_{i=1}^{3}\frac{\theta_i/T}{\exp\left(\theta_i/T\right)-1}\right) \quad (17)$$

Heat capacity of various species (i = N_2/O_2/H_2O):
$$C_{V,i} = N_i k\left(f_i/2+\sum\left(\left(\theta_i/T\right)^2\exp\left(\theta_i/T\right)\Big/\left(\exp\left(\theta_i/T\right)-1\right)^2\right)\right)$$
(18)

The initial conditions of the ODEs are as follows: at t = 0, R = R_o, dR/dt = 0, N_w = 0, Q = 0, T = T_0. Thermodynamic data for various species is given in Table 1. The thermal conductivity and diffusion coefficient (transport parameters for the heat and mass transfer) are determined using Chapman–Enskog theory using Lennard–Jones 12–6 potential at the

bulk temperature of the liquid medium [23–26]. As the time scale for the diffusion of gases is much higher than the time scale of bubble dynamics, this model ignores the diffusion of gas across bubble interface. The ODEs in the bubble dynamics model are solved simultaneously using Runge–Kutta adaptive step size method [27]. Various parameters used in the simulation of bubble dynamics equation (air bubble) and their numerical values are as follows: ultrasound frequency (f) = 40 kHz; ultrasound pressure amplitude (P_A) = 150 kPa; bubble radius (R_o) = 5 μm and 10 μm; water vapor pressure = 2500 Pa (calculated using Antoine type correlation). Various physical properties of water are as follows: density (ρ_L) = 1000 kg/m^3, kinematic viscosity (ν) = 10^{-6} Pa–s, surface tension (σ) = 0.072 N/m and velocity of sound (c) = 1481 m/s.

Physical effect of ultrasound: Ultrasound propagates through the medium in the form of longitudinal wave with series of compression and rarefaction, and causes rapid oscillatory motion of fluid elements called as microstreaming. This motion gives rise to intense micro–mixing in the medium. The magnitude of the microstreaming velocity is given by: $u = P_A/\rho c$. Substituting values of P_A as 1.5×10^5 Pa, ρ = 1000 kg/m^3, and c = 1481 m/s, gives u = 0.101 m/s.

Sonochemical effect of cavitation bubbles: The numerical solution of bubble dynamics model predicts the temperature, pressure and the number of gas & solvent molecules in the bubble at transient collapse. At transient collapse, temperature and pressure reach in extreme conditions, which result dissociation of molecules to form various chemical species. To calculate the composition of the bubble at the time of collapse, we assume that thermodynamic equilibrium is attained [28]. The equilibrium mole fraction of different chemical species in the bubble at the peak conditions reached at transient collapse is estimated using Gibbs free–energy minimization technique [29]. The radial motion of cavitation bubbles generates intense convection in the medium through two phenomena [Eqn. 19-20]:

(i) Micro–convection [30]: $$V_{turb}(r,t) = \frac{R^2}{r^2}\left(\frac{dR}{dt}\right) \quad (19)$$

(ii) Shock waves (or Acoustic waves) [31,32]: $$P_{AW}(r,t) = \frac{\rho_L}{4\pi r}\frac{d^2V_b}{dt^2} = \rho_L \frac{R}{r}\left[2\left(\frac{dR}{dt}\right)^2 + R\frac{d^2R}{dt^2}\right] \quad (20)$$

Where, V_b is the volume of the bubble. A representative value of r is taken as 1 mm. In bubble dynamic model, direct estimation of initial bubble radius is very difficult. Several phenomena such as rectified diffusion, fragmentation of the bubble etc. cause continuous change in this parameter. In a multi–bubble system, a large variation in this parameter may be expected. In order to investigate the influence of this parameter, two numerical values for this parameter, viz. 5 and 10 μm, are selected for this present study. The equilibrium composition of the bubble contents was determined using the FactSage software [33], which is based on the free–energy minimization algorithm proposed by Eriksson [29].

Table 1. Thermodynamic data for various species (data taken from ref. [23–25])

Species	Degrees of freedom (translational + rotational) (f_i)	Lennard–Jones force constants		Characteristic vibrational temperatures θ (K)
		σ (10^{-10} m)	ε/k (K)	
N_2	5	3.68	92	3350
O_2	5	3.43	113	2273
H_2O	6	2.65	380	2295, 5255, 5400

3. Results and Discussion

We would like to mention that no external calcination was applied to the solid particle after the sonication. The product was characterized using Xray powder diffractometer (Bruker, Advanced D8) with monochromatic Cu–K_α (λ=1.5406 Å) radiation operated in the range from 20 to 70^o. The mean crystallite particle size (D_{xrd}) of the product was calculated from the most intense peak (311) using Debye–Scherrer equation [34,35]: $D_{xrd} = 0.9\lambda/(\beta\cos\theta)$, where, λ is the X–ray wavelength, β is the half width of the relevant diffraction peak; θ is the Bragg's angle. The morphology of the nano–particles was determined using field emission scanning electron microscope (FE–SEM, Model: SIGMA VP, Make: Carl Zeiss Microscopy GmbH, Germany). The experimental results are presented in Figs. 1 and 2. The FE–SEM micrograph of the as–synthesized ferrite particles are shown in Fig. 1a and 1b. It could be seen that the ferrite particles are more or less spherical in shape and with narrow size distribution.

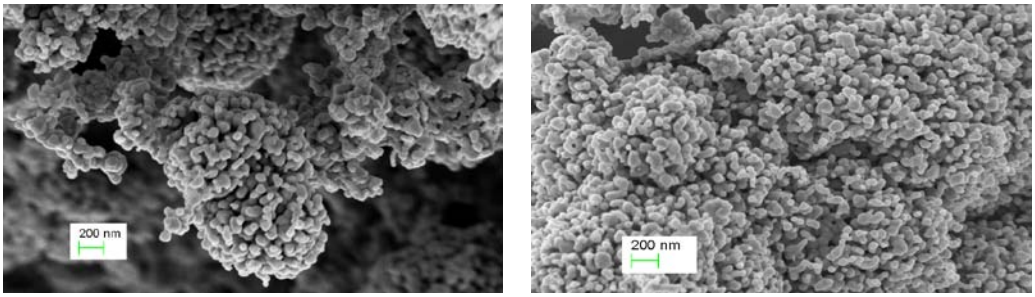

(a) $MnFe_2O_4$ (b) $CoFe_2O_4$

Fig. 1. Field emission scanning electron microscopic (FE–SEM) images of manganese ferrite and cobalt ferrite

The X–ray diffractogram of the solid product obtained after sonication is given in Fig. 2. Fig. 2 shows the diffraction peaks corresponding to the characteristics crystallographic planes of the spinel structure of ferrites [(112), (220), (311), (400), (422), (440)]. These miller indices indicate the single phase ferrites with face–centered cubic (FCC) crystal [36]. The average crystal size of the particles was calculated using Debye–Scherrer equation and it has been found to be 39 nm and 24 nm for $MnFe_2O_4$ and $CoFe_2O_4$, respectively. It should be noted that the ferrite nano–particles are formed during sonication itself, without any external calcination of the material. This essentially indicates the hypothesis of in–situ micro–calcination of the oxide precursors induced due to the energetic collisions between the particles, as they get drifted in high pressure amplitude shock wave generated by the cavitation bubble during transient collapse.

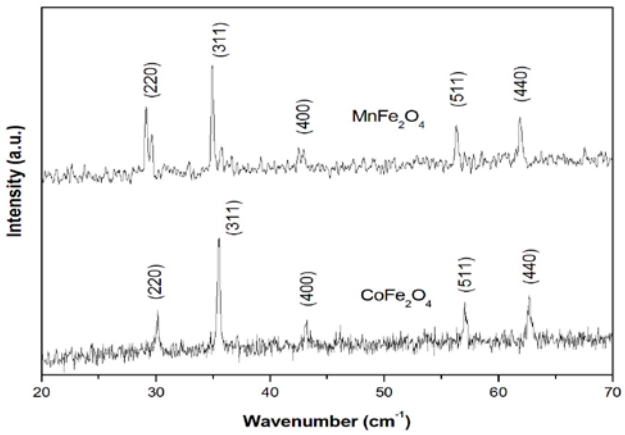

Fig. 2. XRD results of manganese ferrite and cobalt ferrite (without any external calcination)

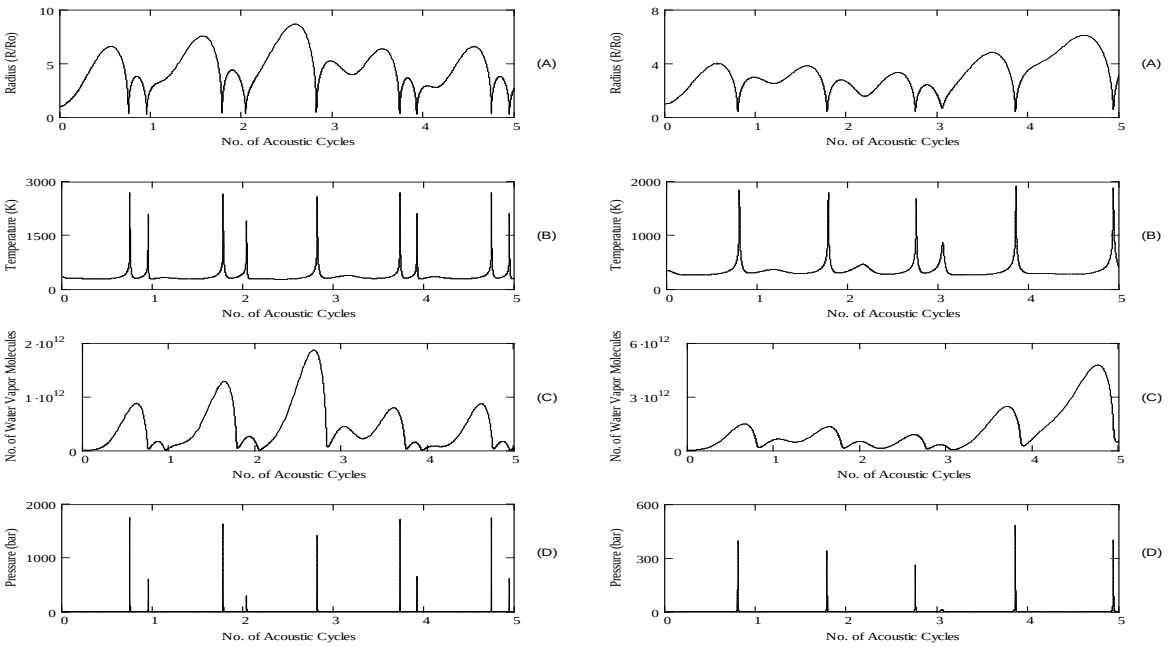

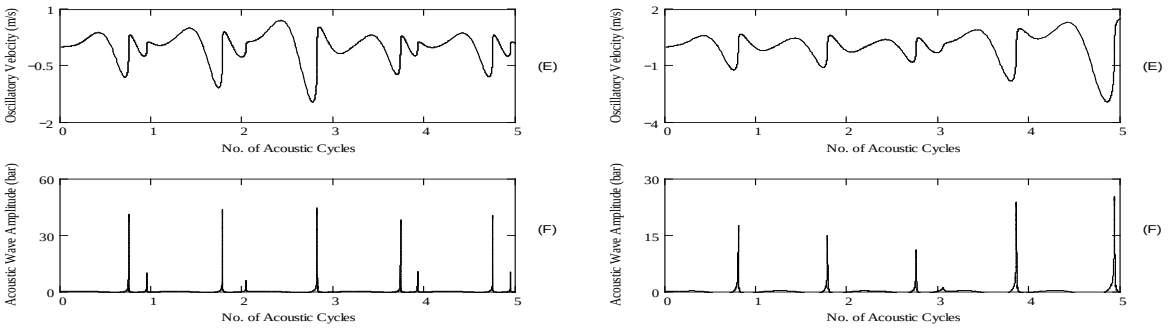

A.1 A.2

Fig. 3. Simulations of radial motion of 5 micron air bubble in water (A.1) and 10 micron air bubble in water (A.2). f = 20 kHz; P_A= 150 kPa; P_o= 101.3 kPa (atmospheric). Time history of (A) radius of the bubble; (B) temperature inside the bubble; (C) water vapor evaporation in the bubble; (D) pressure inside the bubble; (E) microturbulence generated by the bubble; (F) acoustic waves emitted by the bubble.

The simulation results of the bubble dynamic model are presented in Fig. 3, while the equilibrium composition of bubble contents is given in Table 2. The results of the bubble dynamic model shown in Table 2 also give an estimation of the temperature and pressure during the first collapse of the bubble. It could be seen from Table 2 that the number of water molecules in the bubble at the first collapse are 4–15 times higher than the number of gas molecules; and this is because, at the bubble interface the evaporation and diffusion of water vapor in the bubble is proportional to the vapor pressure of water, as a result a large amount of water vapor enters into bubble during expansion and gets entrapped in the consequent collapse phase. Also at the extreme conditions of the bubble, the temperatures reached at 2683 and 1844 K for 5 and 10 µm bubbles, respectively. These temperatures are quite high, which causes in–situ micro–calcination of the metal oxides. That is why no external calcination is needed for formation of ferrite nano–particles. The temperature peaks for 5 µm bubble are higher than that of for 10 µm bubble. This can be attributed to the higher expansion of 5 µm bubble during the rarefaction cycle of ultrasound, as a result of which it undergoes more intense collapse during cavitation. Table 2 also gives the magnitude of the shock waves and the velocity of the micro–turbulence generated by the bubble. The micro–convection velocity for 10 µm is two folds higher than the micro–convection velocity for 5 µm.

Table 2. Summary of simulation results at the first collapse of bubbles (air bubble)

Conditions at the first collapse of the bubble	
5 µm air bubble	10 µm air bubble
T_{max} = 2683 K	T_{max} = 1844 K
P_{max} = 175.3 MPa	P_{max} = 39.72 MPa
V_{turb} = 1.083 m/s	V_{turb} = 2.204 m/s
P_{AW} = 4.097 MPa	P_{AW} = 1.751 MPa
N_{N2} = 1.13 E+10	N_{N2} = 8.07 E+10
N_{O2} = 3.02 E+09	N_{O2} = 2.15 E+10
N_W = 8.17 E+10	N_W = 3.41 E+11

Table 3. Summary of equilibrium composition of species in the bubble at the first collapse

	Equilibrium composition of species in the bubble at collapse	
Species	5 µm air bubble	10 µm air bubble
N_2	1.16×10^{-1}	1.81×10^{-1}
O_2	2.83×10^{-2}	4.73×10^{-2}
H_2O	2.80×10^{-2}	7.69×10^{-1}
O	5.69×10^{-5}	1.99×10^{-6}
H	2.57×10^{-6}	–
O_3	2.28×10^{-7}	–
H_2	2.29×10^{-5}	1.42×10^{-5}
OH	8.08×10^{-4}	3.92×10^{-4}
HO_2	4.22×10^{-5}	1.16×10^{-5}
H_2O_2	4.60×10^{-6}	3.56×10^{-6}
NO	4.57×10^{-3}	1.17×10^{-3}
NO_2	1.11×10^{-4}	2.37×10^{-5}
N_2O	8.69×10^{-6}	–
HNO	9.69×10^{-7}	–

HNO_2	1.76×10^{-5}	5.29×10^{-6}

4. Conclusion

In this study, we have presented the additives free sonochemical route for synthesis of ferrite nano–particles. Under the ultrasound irradiation, the metal acetates as precursors are hydrolyzed and oxidized to form metal oxides. High energy collisions between the particles due to the shock waves generated by transient collapse of cavitation bubble causes synthesis of ferrites through in–situ micro–calcination of the oxide particles. Most notably, no external calcination is needed for formation of ferrites. Experimental results showed that spinel crystalline structure ferrite nano–paticles can be synthesized using only sonochemical method. We believe that results of this preliminary study could form useful guidelines for further research in the area of sonochemical synthesis of nano–sized ferrites.

5. References

[1] E.C. Snelling, Soft Ferrites: Properties and Applications, 2nd ed., *Butterworth Publishing*, London, 1989.

[2] D.C. Jiles, Introduction to Magnetism and Magnetic Materials, 2nd ed., *Chapman and Hall*, London, 1991.

[3] M.A. Willard, L.K. Kurihara, E.E. Carpenter, S. Calvin, and V.G. Harris, "Chemically prepared magnetic nanoparticles", *Int. Mater. Rev. Vol.*, Vol. 49, pp. 125–170, 2004.

[4] B.G. Toksha, S.E. Shirsath, S.M. Patange, and K.M. Jadhav, "Structural investigations and magnetic properties of cobalt ferrite nanoparticles prepared by sol–gel auto combustion method", *Solid State Commun.*, Vol. 147, pp. 479–483, 2008.

[5] K. Winiarska, I. Szczygieł, and R. Klimkiewicz, "Manganese-zinc ferrite synthesis by the sol−gel autocombustion method. Effect of the precursor on the ferrite's catalytic properties", *Ind. Eng. Chem. Res.*, Vol. 52, pp. 353−361, 2013.

[6] Y. Ahn, E.J. Choi, S. Kim, and H.N. Ok, "Magnetization and Mossbauer study of cobalt ferrite particles from nanophase cobalt iron carbonate", *Mater. Lett.*, Vol. 50, pp. 47–52, 2001.

[7] D.O. Yener and H. Giesche, "Synthesis of pure and manganese–, nickel–, and zinc doped ferrite particles in water–in–oil microemulsions", *J. Am. Ceram. Soc.*, Vol. 84, pp.1987–1995, 2001.

[8] Y. Lee, J. Lee, C.J. Bae, J. Park, H. Noh, J. Park, and T. Hyeon, "Large–scale synthesis of uniform and crystalline magnetite nanoparticles using reverse micelles as nanoreactors under reflux conditions", *Adv. Funct. Mater.*, Vol. 15, pp. 503–509, 2005.

[9] S.H. Xiao, W.F. Jiang, L.Y. Li, and X.J. Li, "Low–temperature auto–combustion synthesis and magnetic properties of cobalt ferrite nano–powder", *Mater. Chem. Phys.*, Vol. 106, pp. 82–87, 2007.

[10] I. Elahi, R. Zahira, K. Mehmood, A. Jamil, and N. Amin, "Co–precipitation synthesis, physical and magnetic properties of manganese ferrite powder", *Afr. J. Pure Appl. Chem.*, Vol. 6, pp. 1–5, 2012.

[11] M. Sivakumar, A. Gedanken, W. Zhang, Y.W. Du, D. Bhattacharya, Y. Yeshurun, and I. Felner, "Nanophase formation of strontium hexaferrite fine powder by the sonochemical method using $Fe(CO)_5$", *J. Magn. Magn. Mater.*, Vol. 268, pp. 95–104, 2004.

[12] B.R. Reddy, T. Sivasankar, M. Sivakumar, and V.S. Moholkar, "Physical facets of ultrasonic cavitational synthesis of zinc ferrite particles", *Ultrason. Sonochem.*, Vol. 17, pp. 416–426, 2010.

[13] K.D. Bhatte, D.N. Sawant, D.V. Pinjari, A.B. Pandit, and B.M. Bhanage, "One pot green synthesis of nano sized zinc oxide by sonochemical method", *Mater. Lett.*, Vol. 77, pp. 93–95, 2012.

[14] H.A. Choudhury, A. Choudhary, M. Sivakumar, and V.S. Moholkar, "Mechanistic investigation of the sonochemical synthesis of zinc ferrite", *Ultrason. Sonochem.*, Vol. 20, pp. 294–302, 2013.

[15] T.J. Mason and J.P. Lorimer, "Applied sonochemistry – the uses of power ultrasound in chemistry and processing", *J. Chem. Technol. Biotechnol.*, Vol. 79, pp. 207–208, 2004.

[16] K.S. Suslick, Ultrasound: Its chemical, physical and biological Effects, *VCH*, New York, 1998.

[17] C. Gong and D.P. Hart, "Ultrasound Induced Cavitation and Sonochemical Yields", *J. Acoust. Soc. Am.*, Vol. 104, pp. 2675–2682, 1998.

[18] R. Toegel, B. Gompf, R. Pecha, and D. Lohse, "Does water vapor prevent upscaling sonoluminescence?", *Phys. Rev. Lett.*, Vol. 85, pp. 3165–3168, 2000.

[19] B.D. Storey and A.J. Szeri, "Water vapor, sonoluminescence and sonochemistry", *Proc. R. Soc. Lond. Ser. A*, Vol. 456, pp. 1685–1709, 2000.

[20] J.B. Keller and M.J. Miksis, "Bubble oscillations of large amplitude", *J. Acoust. Soc. Am.*, Vol. 68, pp. 628–633, 1980.

[21] S. Chakma and V.S. Moholkar, "Mechanistic features of ultrasonic desorption of aromatic pollutants", Chem. Eng. J., Vol. 175, pp. 356–367, 2011.

[22] S. Chakma and V.S. moholkar, "Physical mechanism of sono–Fenton process", *AIChE J.*, doi:10.1002/aic.14150, 2013.

[23] J.O. Hirschfelder, C.F. Curtiss, and R.B. Bird, Molecular Theory of Gases and Liquids, *Wiley*, New York, 1954.

[24] E.U. Condon and H. Odishaw, Handbook of physics, *McGraw Hill*, New York, 1958.

[25] R.C. Reid, J.M. Prausnitz, and B.E. Poling, Properties of gases and liquids, *McGraw Hill*, New York, 1987.

[26] R.B. Bird, W.E. Stewart, and E.N. Lightfoot, Transport phenomena, 2nd ed., *Wiley*, New York, 2001.

[27] W.H. Press, S.A. Teukolsky, B.P. Flannery, and W.T. Vetterling, Numerical Recipes, 2nd ed., *Cambridge University Press*, New York, 1992.

[28] J.S. Krishnan, P. Dwivedi, V.S. Moholkar, “Numerical investigation into the chemistry induced by hydrodynamic cavitation”, *Ind. Eng. Chem. Res.*, Vol. 45, pp. 1493–1504, 2006.
[29] G. Eriksson, “Thermodynamic studies of high temperature equilibria—XII: SOLGAMIX, a computer program for calculation of equilibrium composition in multiphase systems”, *Chem. Scr.*, Vol. 8, pp. 100–103, 1975.
[30] Y.T. Shah, A.B. Pandit, and V.S. Moholkar, Cavitation reaction engineering, *Plenum Press*, New York, 1999.
[31] S. Grossmann, S. Hilgenfeldt, M. Zomack, and D. Lohse, “Sound radiation of 3 MHz driven gas bubbles”, *J. Acoust. Soc. Am.*, Vol. 102, pp. 1223–1227, 1997.
[32] V.S. Moholkar and M.M.C.G. Warmoeskerken, “An integrated approach to optimization of an ultrasonic processor”, *AIChE J.*, Vol. 49, pp. 2918–2932, 2003.
[33] FactSage software, http://www.factsage.com/, access on June– 2013.
[34] V. Drits, J. Srodon, and D.D. Eberl, “XRD measurement of mean crystallite thickness of illite an illite/smectite: reappraisal of the kubler index and the scherrer equation”, *Clay. Clay Miner.*, Vol. 45, pp. 461–475, 1997.
[35] Y. Koseoglu, F. Alan, M. Tan, R. Yilgin, and M. Ozturk, “Low temperature hydrothermal synthesis and characterization of Mn doped cobalt ferrite nanoparticles”, *Ceramic. Int.*, Vol. 38, pp. 3625–3634, 2012.
[36] M.G. Naseri, E.B. Saion, H.A. Ahangar, A.H. Shaari, and M. Hashim, “Simple synthesis and characterization of cobalt ferrite nanoparticles by a thermal treatment method”, *J. Nanomater.*, ID 907686, pp. 1–8, 2010.